Bright Breathers in Nonlinear Left-Handed Metamaterial Lattices

V. Koukouloyannis,[1,2,3] P. G. Kevrekidis,[1] G. P. Veldes,[4,5]
D. J. Frantzeskakis,[4] D. DiMarzio,[6] X. Lan,[6] and V. Radisic[6]

[1]*Department of Mathematics and Statistics, University of Massachusetts, Amherst MA 01003-4515, USA*
[2]*Department of Mathematics, Statistics and Physics, College of Arts and Sciences, Qatar University, P.O. Box 2713, Doha, Qatar*
[3]*Faculty of Civil Engineering, School of Engineering, Aristotle University of Thessaloniki, 54249, Thessaloniki, Greece*
[4]*Department of Physics, National and Kapodistrian University of Athens, Panepistimiopolis, Zografos, Athens 15784, Greece*
[5]*Department of Electronics Engineering, Technological Educational Institute of Central Greece, Lamia 35100, Greece*
[6]*NG Next, Northrop Grumman Corporation, One Space Park, Redondo Beach, CA 90278 USA*

In the present work, we examine a prototypical model for the formation of bright breathers in nonlinear left-handed metamaterial lattices. Utilizing the paradigm of nonlinear transmission lines, we build a relevant lattice and develop a quasi-continuum multiscale approximation that enables us to appreciate both the underlying linear dispersion relation and the potential for bifurcation of nonlinear states. We focus here, more specifically, on bright discrete breathers which bifurcate from the lower edge of the linear dispersion relation at wavenumber $k = \pi$. Guided by the multiscale analysis, we identify such solutions in a numerically exact (up to a prescribed accuracy) way for both the stable inter-site centered and the unstable site-centered members of the relevant family. We quantify the associated stability via Floquet analysis and the Peierls-Nabarro barrier of the energy difference between these branches. Finally, we explore the dynamical implications of these findings towards the potential mobility or lack thereof (pinning) of such breather solutions.

I. INTRODUCTION

A major thrust of theoretical and experimental studies within electromagnetic media in the last fifteen years has been allocated to the study of artificially engineered, so-called metamaterial structures [1–3]. Among them, left-handed metamaterials (LHMs) feature (in specific frequency bands) simultaneously negative effective permittivity and permeability, still resulting in a real propagation speed. The consequent feature of opposite directions of transmission of energy and wavefronts (or of antiparallel group and phase velocities) has been examined at microwave, as well as optical frequencies [4–6].

On the other hand, from the nonlinear science perspective, the same time frame has seen an explosion of interest in structures that are time-periodic and exponentially localized in space, the so-called discrete breathers [7, 8]. The experimental relevance of these entities in contributing to the localization of energy has been recognized in a broad and diverse array of settings. These range from micro-mechanical cantilever arrays [9, 10], and torsionally-coupled pendula [11] to electrical transmission lines [12]. They also extend to Josephson junction superconducting arrays [13, 14], coupled antiferromagnetic layers [15], halide-bridged transition metal complexes [16] and, more recently, to material science themes such as granular crystals [17, 18]. It should also be added that discrete breathers have also been predicted to occur in nonlinear magnetic metamaterials composed by split-ring resonators (SRRs) [19] (see also the review [20] and references therein).

Our aim in the present work is to explore a prototypical case example of the interface between these two booming fields, utilizing the framework of transmission line (TL) theory. This is a method that has been widely used for the study of LHMs [21, 22]. Here, the direct connection of electromagnetic properties is between the effective permittivity ϵ and permeability μ of the LHM and, respectively, the serial and shunt impedance of the TL model. Our particular focus will be on the nonlinear LHMs where the dependence of the impedances on the voltage (or of the effective permittivity/permeability properties on the electromagnetic field) generates a wealth of relevant phenomenology. This has been widely explored via the embedding of wires and SRRs into nonlinear dielectrics [23, 24], as well as via the embedding of diodes into elements such as the SRRs [25–27]. A broad array of studies have focused on the TL description and its ability to feature nonlinear structures; see, e.g., the review of [28]. More recent theoretical works have also utilized the framework of the nonlinear Schrödinger (NLS) equation, enabling the description of bright [29] or dark [30] solitons, which have been observed in experiments.

In our specific example of interest, a TL-analogue of a left-handed medium is explored, as an extension of our earlier considerations [31]. These were, at least in part, motivated by the development of strongly nonlinear and voltage symmetric barium strontium titanate (BST) thin film capacitors [32]. This symmetric dependence of the capacitance of the left-handed element on the voltage has been appropriately incorporated in our analysis. Our aim herein is to go a significant step further than previous studies in establishing the existence, stability, physical relevance

and dynamical properties of discrete breathers in such systems. In earlier works, to the best of our knowledge, upon development of the relevant TL model, NLS-model reductions were used to identify an initial ansatz of an approximate soliton solution and subsequently these were used in the original dynamical lattice to assess their potential robustness. Here, we do not restrict our considerations to that. We use the NLS to assess the linear properties and (weakly) nonlinear potential of the model to carry suitable excitations. Yet, we then go on to compute *numerically exact* (up to a prescribed accuracy) nonlinear bright breather solutions and assess their spectral stability, using Floquet theory. We identify both stable solutions (centered between adjacent lattice sites) and unstable ones (centered on a lattice site) and quantify their energy difference (the celebrated Peierls-Nabarro (PN) barrier [36]). Finally, we explore the dynamical implications of our stability conclusions by initializing the unstable solutions with a perturbation bearing a component along this unstable eigendirection. We observe how the solutions transition from a situation of high mobility when the PN barrier is low, to one of low mobility and eventual trapping/pinning between two adjacent lattice sites.

Our presentation is structured as follows. In section II, we present the model and its theoretical analysis, including the quasi-continuum approximation leading to an approximate NLS waveform emulating the breather state. Then, in section III, we validate and extend the relevant results via detailed numerical computations, identifying the two families of breather solutions, exploring their stability and dynamics. Finally, in section IV, we summarize our findings and present some conclusions for future work.

II. MODEL AND THEORETICAL ANALYSIS

A. The Model

Following up on our earlier work [31], we build a lattice of coupled units, each of which constitutes a nonlinear nodal element, as shown in Fig. 1. 1

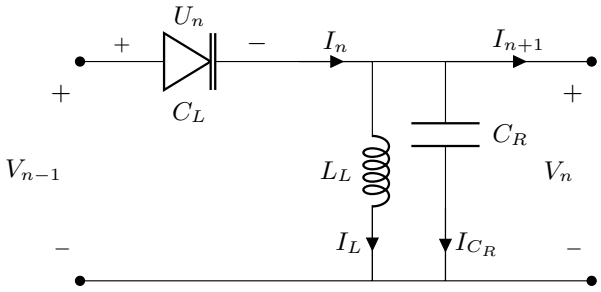

FIG. 1: A sketch of the unit cell of the transmission line emulating the left-handed metamaterial.

Kirchhoff's laws for this unit element circuit read

$$I_n = I_L + I_{C_R} + I_{n+1}, \tag{1}$$
$$U_n = V_{n-1} - V_n. \tag{2}$$

Taking into regard that

$$I_n = \frac{d}{dt}(C_L(U_n)\,U_n), \quad I_{n+1} = \frac{d}{dt}(C_L(U_{n+1})\,U_{n+1}), \quad I_{C_R} = \frac{d}{dt}(C_R V_n),$$

substitution to Eqs. (1)-(2) yields:

$$L_L \frac{d^2}{dt^2}\left[C_L(U_n)\,U_n - C_L(U_{n+1})\,U_{n+1}\right] - L_L C_R \frac{d^2}{dt^2}\left(V_n\right) - V_n = 0, \tag{3}$$

where we have used also $L_L \dfrac{dI_L}{dt} = V_n$. We have thus expressed the dynamical model as a second-order dynamical equation modeling the voltages along the TL.

Motivated by the barium strontium titanate (BST) thin film capacitors of [32] which feature a strongly nonlinear symmetric dependence on the voltage, we explore a dependence of C_L from U_L which is symmetric i.e., $C(U) =$

$C_0 + \alpha U^2$. Thus, Eq. (3) becomes:

$$L_L C_0 \frac{d^2}{dt^2}\left[V_{n-1} - 2V_n + V_{n+1}\right] - L_L C_R \frac{d^2 V_n}{dt^2} - V_n + \alpha L_L \frac{d^2}{dt^2}\left[(V_{n-1} - V_n)^3 - (V_n - V_{n+1})^3\right] = 0.$$

To express the above equation in dimensionless units, we measure time in $1/\omega_0 = \sqrt{L_L C_0}$ and voltage in units of $\sqrt{C_0/\alpha}$, so that the above equation becomes

$$\frac{d^2}{dt^2}(V_{n-1} - 2V_n + V_{n+1}) - g\frac{d^2 V_n}{dt^2} - V_n + \frac{d^2}{dt^2}[(V_{n-1} - V_n)^3 - (V_n - V_{n+1})^3] = 0, \tag{4}$$

where $g = C_R/C_0$. In what follows the parameter g will be assumed to lie in the the interval $g \in (0, 3.5)$, which will play a critical role for the existence of bright breathers in this system.

It is now useful, for the purposes of our analytical and numerical considerations, to adopt experimentally relevant parameter values. Left-handed metamaterials featuring the equivalent lattice model of Fig. 1 can be fabricated in planar structures using lumped elements, or distributed components, in microwave frequencies. In this case, the values of electrical parameters of equivalent lattice model, namely the capacitances and inductances can be extracted from the physical parameters of these structures [33]. For instance, for an array of complementary SRRs (CSRRs) [34], depending on the size of these resonant elements, and the type of the diode that is inserted in the slits of the CSRRs, one can use the following parameter values. In the case of relatively small CSRRs, operating in the microwave frequency range 1.77 GHz $< f <$ 2.7 GHz, one may use a varactor diode MA46H146 [35], and obtain: $C_0 \approx 0.5$ pF, $L_L \approx 2.3$ nH, and $C_R \approx 1.5$ pF; this choice leads to $g \simeq 3$. On the other hand, in the case of relatively large CSRRs, operating in the frequency range 130 MHz $< f <$ 1.100 MHz, one may use a barium strontium titanate (BST) thin film capacitor [32], and obtain: $C_0 \approx 80$ pF, $L_L = 4.7$ nH and $C_R = 4.5$ pF; this results in $g \simeq 0.056$.

B. Energy of the system

Here, we will introduce the energy of the system for a number of both theoretical and practical reasons. On the one hand, the total energy is a conserved quantity in the system and yields a practical diagnostic for the accuracy, e.g., of the numerical simulations performed below. On the other hand, its density is a measure of the localization of the coherent structures (breathers) that we will consider in what follows. Hence, the energy density provides an intrinsic quantity tailored towards monitoring the space-time dynamical evolution of the system.

Considering from first principles, the energy in the different capacitive and inductive elements, we can reconstruct the energy of the unit-cell of the lattice. This is given by

$$E_u = E_{C_L} + E_{C_R} + E_{L_L}.$$

For the specific form of $C_L - U$ dependence, this becomes

$$E_u = \frac{1}{2}C_0 U^2 + \frac{3}{4}\alpha U^4 + \frac{1}{2}C_R V_n^2 + \frac{1}{2}L_L I_L^2. \tag{5}$$

Measuring the energy in units of C_0^2/α, (and also time in $1/\omega_0 = \sqrt{L_L C_0}$ units, voltage in units of $\sqrt{C_0/\alpha}$, as before and current in units of $C_0/\sqrt{\alpha L_L}$), Eq. (5) in its rescaled dimensionless form becomes:

$$E_u = \frac{1}{2}U^2 + \frac{3}{4}U^4 + \frac{g}{2}V_n^2 + \frac{1}{2}I_L^2. \tag{6}$$

The total (conserved) energy of the lattice is then reconstructed upon the relevant summation over nodes:

$$E_{tot} = \sum_n \left\{\frac{1}{2}(V_n - V_{n+1})^2 + \frac{3}{4}(V_n - V_{n+1})^4 + \frac{g}{2}V_n^2 + \frac{1}{2}I_{L_n}^2\right\}. \tag{7}$$

We can also define the "energy per site" as

$$E_n = \frac{1}{4}\left[(V_{n-1} - V_n)^2 + (V_n - V_{n+1})^2\right] + \frac{3}{8}\left[(V_{n-1} - V_n)^4 + (V_n - V_{n+1})^4\right] + \frac{g}{2}V_n^2 + \frac{1}{2}I_{L_n}^2, \tag{8}$$

such that $E_{tot} = \sum_n E_n$.

C. The quasi-continuum approximation

The mathematical model of Eq. (4) is less straightforward to tackle directly. It is for this reason that we employ a quasi-continuum approximation [40]. This affords us an understanding of both the underlying linear band structure and that of developing the weakly nonlinear theory, based on the NLS approximation.

More concretely, we seek solutions of Eq. (4) in the form of the asymptotic expansion:

$$V_n = \sum_{\ell=1}^{+\infty} \epsilon^\ell V_\ell(X,T) e^{i\ell(\omega t - kn)} + \text{c.c.}, \tag{9}$$

where c.c. stands for complex conjugate, and V_ℓ are unknown envelope functions, depending on the slow variables:

$$X = \epsilon(n - v_g t), \qquad T = \epsilon^2 t, \tag{10}$$

with v_g being the group velocity, as can be found self-consistently from the linear dispersion relation (see below). The scaling selected here is the standard one associated with the NLS model. Finally, ω and k denote the carrier's frequency and wavenumber, respectively, and ϵ is a formal small parameter, characterizing the amplitude of the solution (and its inverse spatial width).

The resulting equations from the multiscale expansion order by order read (cf. also Ref. [31]):

$$O(\epsilon^1) \ : \ \frac{1}{\omega^2} = 2 + g - 2\cos k; \tag{11}$$

$$O(\epsilon^2) \ : \ v_g = -\omega^3 \sin k; \qquad V_2 = 0; \tag{12}$$

$$O(\epsilon^3) \ : \ i\partial_T V_1 + P\partial_X^2 V_1 + Q|V_1|^2 V_1 = 0, \quad P = \frac{\omega^3}{2}(\cos k - 3\omega^2 \sin^2 k), \quad Q = -24\omega^3 \sin^4(k/2); \tag{13}$$

$$V_3 = \frac{144\omega^2(1+2\cos k)\sin^4(k/2)V_1^3}{1+g-2\cos(3k)}.$$

The first one of these, at O(ϵ), represents the linear dispersion relation of the LHM. Notice that the dispersion relation (11) suggests that there exist two cutoff frequencies, namely an upper one, $\omega_{max} = 1/\sqrt{g}$ (corresponding to $k = 0$), and a lower one, $\omega_{min} = 1/\sqrt{g+4}$ (corresponding to $k = \pi$); notice that the lower cutoff frequency is due to discreteness since, evidently, this frequency vanishes in the continuum limit.

At the next order, the solvability condition yields the group velocity (the velocity of wavepackets) $v_g = d\omega/dk$, which is not only distinct from the phase velocity $v_p = \omega/k$, but also carries opposite sign, as per the left-handed nature of the medium; this becomes clear by the form of the dispersion relation shown in the left panel of Fig. 2, which features a negative slope. Note that, at the second order, the solvability condition leads to a vanishing contribution $V_2 = 0$, as is commonly the case in such multiscale expansions (under symmetric conditions).

At the third order, we obtain the NLS equation for V_1. Its dispersion and nonlinearity coefficients, P and Q respectively, depend on the frequency, but the latter is slaved to the wavenumber through the dispersion relation. Last, but not least, the third-order reduction/decomposition of the solution is also derived. This enables us to reconstruct the solution up to errors of size ϵ^4. Naturally, we expect this to be a fairly adequate approximation of the solution within the weakly nonlinear regime.

The product PQ determines the "nature" of the resulting NLS. In the region where the relevant quantity is positive, per the standard general theory of the NLS equation [37–39], the dynamics is associated with a self-focusing scenario that supports bright solitons. On the other hand, when $PQ < 0$, then we are in a self-defocusing regime where, e.g., dark solitons may arise. The analytical availability of these waveforms at the NLS level, as well as the explicit form of the transformation allows us to express these potential solutions in the LHM dynamics.

D. Identifying Bright Breathers

In this work we are, more specifically, interested in exploring the existence and stability of bright breather-like solutions. For this purpose, we are going to use the NLS bright soliton solution as initial estimate for the periodic motion finding numerical scheme, which is given by Eq (14).

$$V_1 = \sqrt{\frac{2|P|}{|Q|}} u_0 \,\mathrm{sech}\left(u_0(X - 2c|P|T)\right) \exp[i\left(cX + (u_0^2 - c^2)|P|T\right)], \tag{14}$$

where u_0 and c are free O(1) parameters setting the amplitude/inverse width and wavenumber of the soliton, respectively.

Since we are seeking standing solutions ($u_g = 0$), we require the value of the wavenumber to be $k = 0$ or $k = \pi$, as can be seen by Eq. (12). In addition, since the bright solution is supported in the k-parameter range where the NLS demonstrates focusing behavior, i.e. $PQ > 0$, the appropriate choice of the wavenumber is $k = \pi$, as shown in Fig. 2 where the value of the product PQ is depicted for $g = 0.056$ (in line with what was used in Ref. [31]). More generally, it is well known that the nonlinear solutions will bifurcate from the edges of the linear band. Near the $k = 0$ limit, we can observe that the relevant product vanishes, rendering a corresponding nonlinear waveform bifurcation less promising. However, the focusing nature of the equation near $k = \pi$ is promising towards attempting the profile of Eq. (14), in conjunction with the expansion of Eq. (9) and the variables of Eq. (10), to identify a bright breather profile. We will thus utilize this selection as an initial guess in our attempt to identify numerically exact bright breather solutions for frequencies below those of the linear spectrum lower band edge in what follows.

III. NUMERICAL RESULTS

A. Existence and linear stability of breather families

In order for a breather-like solution to exist it is necessary for its frequency $\omega = 2\pi/T$ to lie outside the range of the dispersion relation (see e.g. fig. 2). In addition, every multiple of this frequency should also avoid this range, in order for the conditions of the theorem for the existence of breathers to be satisfied [41]. Since this solution will bifurcate from the right end of this curve it will lie bellow the curve. As we can easily verify from the top panels of Fig. 2, this in not possible for $g = 0.056$ (which is one of the physically relevant values of g mentioned in the previous section) since the second harmonic of every choice of frequency below the dispersion relation curve will resonate with the linear spectrum for this choice of g. We should note here that in a chain with a few nodes, due to the quantization of the wavenumbers (and the resulting "gaps" within the pass band), these resonances can be avoided. Nevertheless, we do not consider this scenario here, having in mind, in principle, the case of an extended (practically infinite) lattice.

In order to manage to avoid the linear spectrum represented by the dispersion relation of Eq. (11), we have to use a value of g that provides a suitably narrow linear band. For this purpose, we choose the value of $g = 3$ (as mentioned also in the previous section). The corresponding diagrams are shown in the bottom panels of Fig. 2. The limiting values of ω are $\omega_{min} = 0.378$ and $\omega_{max} = 0.577$. Thus, if we consider, e.g., the limiting value $\omega = 0.378$ for the frequency of our breather, then the second harmonic $2\omega = 0.756$ lies above the value of ω_{max} and the conditions for the persistence of the breathers are automatically satisfied [41].

The solution of Eq. (14) for $k = \pi$ is introduced in Eq. (9), together with the third-order contribution V_3 of Eq. (14). Subsequently, the numerical scheme is iterated leading, upon convergence, to the identification of the periodic orbit and the associated period. For this initial estimate and for $T = 16.7 \Rightarrow \omega = 0.376$ we get two distinct breather solutions, namely the onsite and inter-site one. After acquiring the breathers for a particular value of the frequency, we follow a continuation procedure and get two one-parameter families of breathers with ω as the corresponding parameter. The onsite family, for $T = 16.7 - 21.5$ or $\omega = 0.376 - 0.292$ is shown in Fig. 3, together with the corresponding Floquet multipiers λ_i. Using the monodromy matrix and identifying its eigenvalues, as per the well-known numerical technology discussed, e.g., in Ref. [8], we can identify the stability of these solutions. When the λ_i's are all on the unit circle, the corresponding solutions are stable, while pairs on the real axis (exponential growth), or quartets off of the unit circle (oscillatory growth) are associated with instability. The onsite family is linearly unstable since there is always a pair of multipliers leaving the unit circle along the real axis. The value of the largest characteristic exponent μ_i with respect to ω is shown in Fig. 5.

The inter-site family for $T = 16.7 - 21.5$ or $\omega = 0.376 - 0.292$ is shown in Fig. 4. This family is linearly stable *throughout* the relevant frequency range, since all Floquet multipliers lie on the unit circle for all values of ω.

B. Bifurcation from the linear limit

Both the onsite and inter-site families bifurcate from the same linear mode at the band edge of $k = \pi$. This can be seen in two different ways. In Fig. 5, the dependence of the square of the appropriate characteristic exponent μ of the onsite and inter-site families, with respect to the frequency of the breather is shown. The relationship between the characteristic exponents and the corresponding Floquet multipliers is given by $\lambda = e^{\mu T}$. In the upper half-plane of this diagram, the value of the square of the largest real characteristic exponent is shown for the onsite family. In the lower half-plane of the diagram, the square of the value of one of the two isolated characteristic exponents which lie

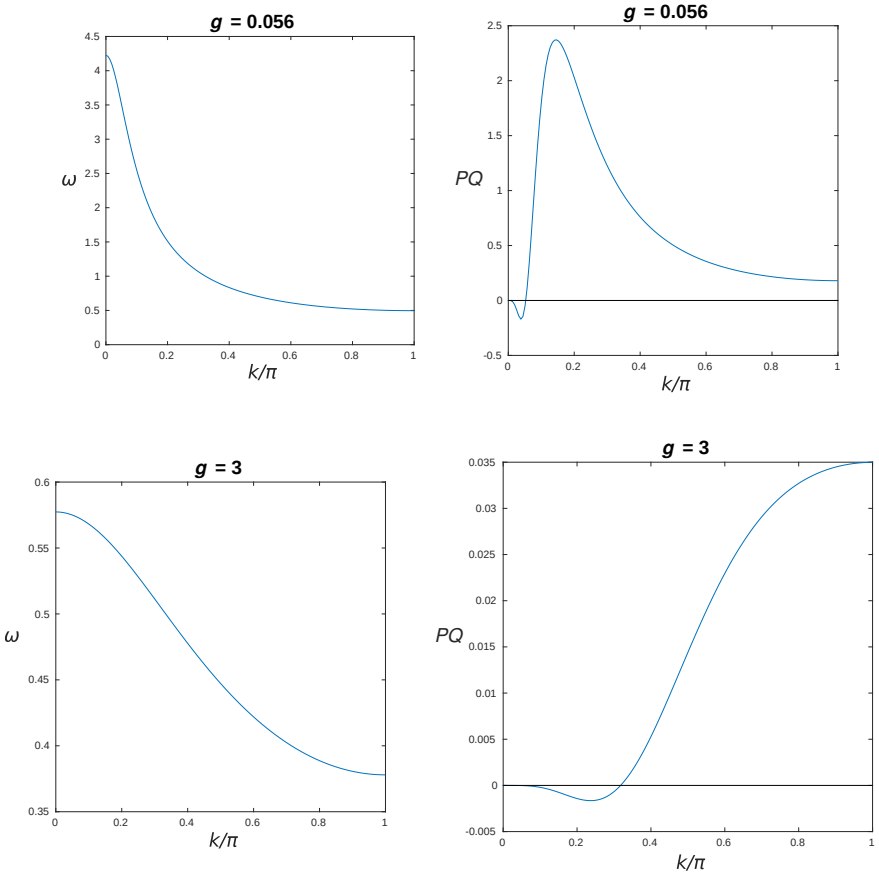

FIG. 2: (Color online) Top left panel: the linear dispersion relation for $g = 0.056$ [cf. Eq. (11)]. Top right panel: the dependence of the factor PQ (which determines the focusing or defocusing nature of the model) on the frequency ω; see also the text. The bottom panels show the same quantities but now for $g = 3$. When $PQ > 0$, the nonlinearity is self-focusing while for the opposite sign, it is self-defocusing.

close to 1 (but on the unit circle), is depicted. Since this exponent is purely imaginary, μ^2 is negative. This confirms the instability of the former and the (spectral) stability of the latter family.

A second way to visualize this bifurcation is to depict the total energy of the lattice (measured in accordance with Eq. (7)) for the two distinct configurations with respect to the frequency of the solution. In Fig. 6 the two resulting curves are shown. The two curves almost coincide and their difference is rather difficult to discern. There is a small divergence in the left part of the diagram. The lower curve corresponds to the inter-site solution. This fact is energetically consistent since the lower energy corresponds to the linearly stable solution (a local energy minimum). The central panel showcases a sub-interval of the entire frequency interval in order to clarify the energy difference. Finally, the right panel shows the energy difference as a function of ω, presenting the rapid growth of this quantity as a function of the frequency. The significant dynamical implications of this rapid growth will be explored in the next subsection.

C. Breather Dynamics

Let us now examine the dynamical behavior of the linearly unstable (onsite) breather solutions under perturbation. For the inter-site waveforms, we have simply confirmed their dynamical stability; in this case, upon weak perturbations, nothing interesting happens. The perturbation we consider for the unstable onsite solutions is one along the direction of the eigenstate, which corresponds to the largest unstable Floquet multiplier of the $T = 19$, $\omega = 0.331$ onsite breather multiplied by a prefactor 0.1. Arguably, there is no single optimal way to perform the relevant perturbation. Here, we opted to perturb all the members of the breather family by the same "kick" (however, even in that case, the kick does not have same projection to the respective unstable eigendirection of each family member).

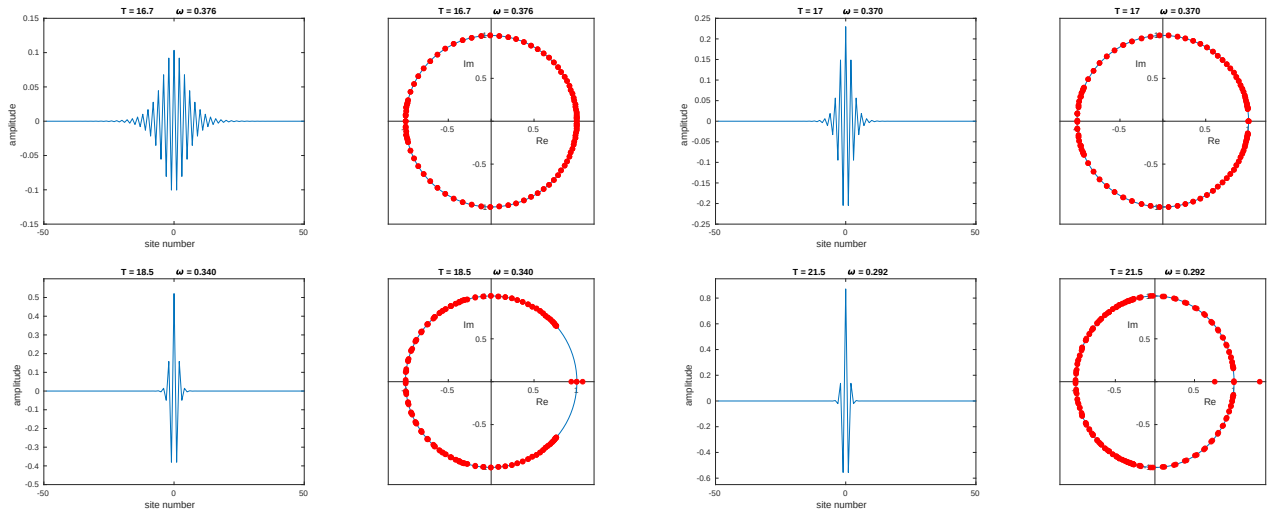

FIG. 3: The onsite family for $T = 16.7 - 21.5$, or $\omega = 0.376 - 0.292$, together with the corresponding Floquet multipiers. We can see here that this family is linearly unstable since there is a pair of multipliers leaving the unit circle along the real axis.

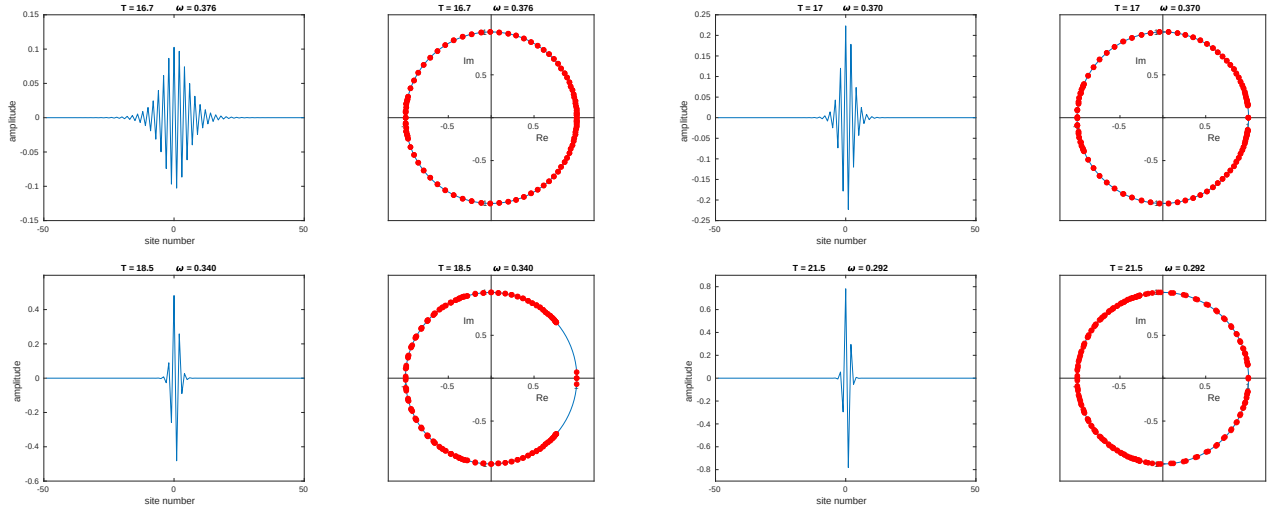

FIG. 4: The intersite family for $T = 16.7 - 21.5$, or $\omega = 0.376 - 0.292$, together with the corresponding Floquet multipiers. We can see here that this family is linearly (spectrally) stable, since all multipliers stay on the unit circle for all values of ω in this interval.

The results of the dynamical simulations are shown in Fig. 7, where the position of the maximum of the energy-per-site is depicted with respect to the time elapsed. In general we observe that under this perturbation the breathers present some mobility. One can think of this as increasing the energy of the saddle point, (by perturbing it along the unstable eigendirection) giving it a kick that allows it to become mobile in the direction connecting the onsite energy maxima with the inter-site energy minima. In the left panel the behavior of the breathers with $T = 17 - 17.4$ is depicted. In this case as we move away from the bifurcation point i.e. for increasing values of the period (decreasing values of the frequency) the mobility of the breather is increased. This happens because as the period is increased more energy is channeled towards the mobility direction since the perturbation used is the one which corresponds to the period value $T = 19$. As the values of the period (frequency) are further increased (decreased), we observe the opposite phenomenon (right panel of Fig. 7), i.e., the breather mobility is decreased. In this case, we are close to the period of which the eigenstate we use for the perturbation. As the period increases further (frequency decreases), the Peierls-Nabarro barrier becomes larger (rapidly so), so the mobility decreases. In particular, for periods $T = 18,\ 18.5$ ($\omega = 0.349,\ 0.34$), we observe a linear increase of the distance of the breather from the center, while for periods $T = 18.9,\ 19$ ($\omega = 0.332,\ 0.331$) the breather moves for some lattice sites and then it stops. Finally, for $T = 19.1$ ($\omega = 0.329$), and all the larger period (smaller frequency) values, the breather does not move at all. Instead, it performs

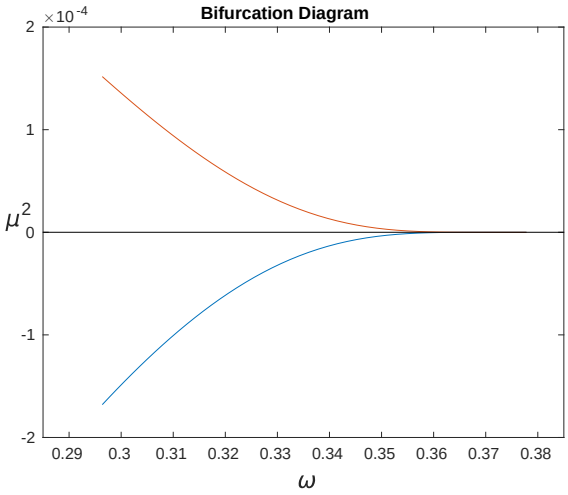

FIG. 5: The dependence of the square of the appropriate characteristic exponent μ of the onsite and inter-site families (see also the discussion in the text), with respect to the frequency of the breather. In the upper half-plane, the value of the square of the largest real characteristic exponent is shown for the onsite family. In the lower half-plane, the square of the value of one of the two isolated characteristic exponents which lie close to 1 (yet on the unit circle), is shown. Since this exponent is purely imaginary, μ^2 is negative. The former characterizes the instability of the onsite branch, while the latter illustrates the spectral stability of the inter-site branch.

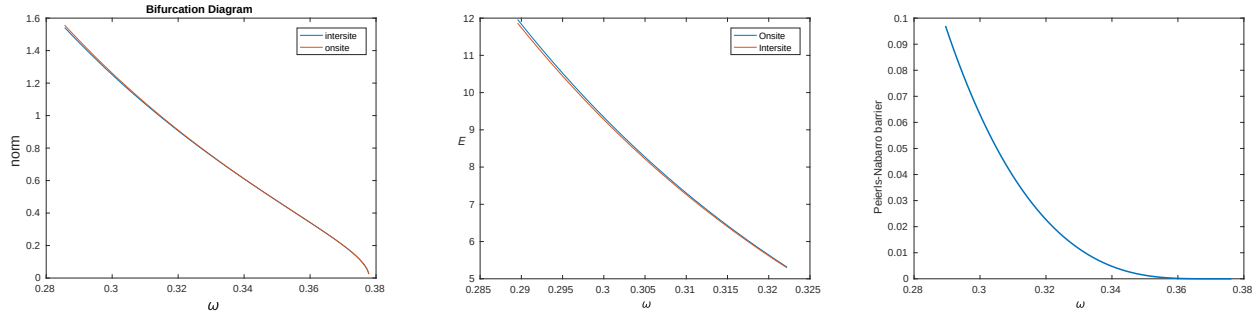

FIG. 6: Left and middle panel: the bifurcation diagram of the total energy of the lattice with respect to the frequency of the breather. The two curves almost coincide. The lower energy curve corresponds to the inter-site solution (local energy minimum) while the higher to the onsite one (saddle point of the energy surface). This fact is energetically consistent with the spectral stability of the former solution and the instability of the latter. In the left panel the curves for the whole range of existence of the breather are shown. In the middle panel a sub-interval of the frequency range is considered in order to more lucidly illustrate the difference between the two curves. The right panel presents the energy difference between the curves (the PN barrier) as a function of the frequency.

a small oscillation around the originating lattice site. This is strongly reminiscent of the dramatically different (in comparison to the continuum) highly discrete behavior originally identified in models such as the sine-Gordon and other Klein-Gordon ones [42, 43], and also explored in other such models, including the discrete nonlinear Schrödinger ones [44].

In Fig. 8, the contour plot of the energy-per-site with respect to the site number and time is shown. This gives a transparent picture of the distribution of the energy, illustrating the transition from high mobility (left panel) to partial mobility (middle panel) and finally to complete trapping and pinning between two lattice sites (right panel). It can be clearly inferred that in the vicinity of the linear limit (the limit where the NLS and multiscale description are accurate), the breather is highly mobile. As the frequency is decreased, the dynamics becomes progressively more discrete and the breathers less mobile.

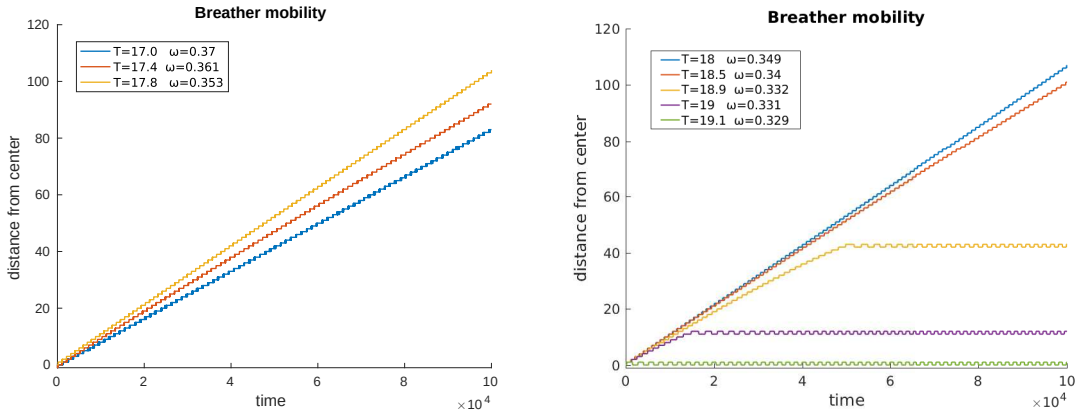

FIG. 7: (Color Online) Breather mobility under perturbation. Left panel: The mobility of the breather increases as the frequency decreases. Right panel: The mobility of the breather decreases as the frequency decreases.

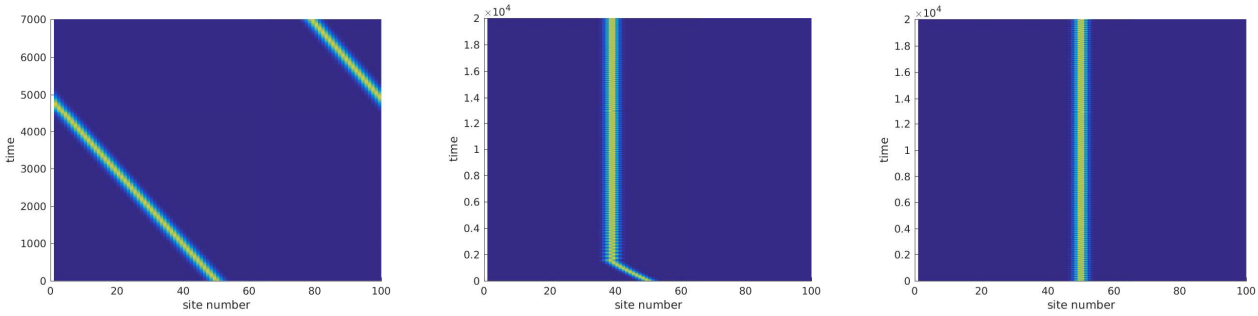

FIG. 8: (Color Online) Contour plots of the energy-per-site with respect to the site number and time are shown. In the left panel, the linear motion of the breather is shown for the case $T = 18.5,\ \omega = 0.34$. The breather passes to the opposite side of the graph because we have considered periodic boundary conditions. Here, the breather energy can be freely transferred within the lattice. In the central panel, the case $T = 19,\ \omega = 0.331$ is considered. The breather moves for some lattice sites and then it stops, being trapped and performing small oscillations around a single local energy minimum (a corresponding inter-site configuration). In the right panel for the $T = 19.3,\ \omega = 0.326$ breather, under the specific perturbation, it is never possible for the breather to traverse the lattice. Instead, it performs only small oscillations around the corresponding local energy minimum intersite configuration.

IV. CONCLUSIONS AND FUTURE CHALLENGES

In the present work, we have systematically examined the possibility of left-handed metamaterial lattices to support discrete breathers. Starting from the underlying nonlinear transmission line model, and unveiling its energy preserving structure, we developed a nonlinear Schrödinger-based multiscale analysis. This formulation operated as a yardstick that revealed both the underlying linear structure, but importantly also revealed the nature of the weakly nonlinear limit. More specifically, it rendered evident that among the two stationary breather limits, the one that was promising for bright breathers was that of $k = \pi$ (i.e., of anti-symmetric nearest neighbor excitations). There, the bright soliton ansatz of the NLS could be used to reconstruct approximate bright breathers of the original (transmission line) lattice model.

Contrary to earlier works simply testing in direct numerical simulations the robustness of such states, here we went a significant step further. We identified the numerically exact solutions and continued them parametrically over the frequency. We revealed that similarly to other models of both kink and breather-bearing type [42–44], the bright breathers herein come in two varieties, namely onsite and inter-site. The detailed numerical linear stability thereof was used to establish that the former solution is unstable and the latter one is stable. Finally, the relevant solutions were used in dynamical evolution numerical experiments confirming that the unstable onsite configurations could, in principle, become mobile. However, this mobility was far more significant for frequencies near the linear limit and was considerably more restricted, as the solutions became more highly nonlinear, and more narrow (far from the linear limit).

This study paves the way for numerous related explorations in the future. We considered here a model where the capacitance increases with the voltage. If instead, the capacitance decreases with the voltage (as is, e.g., the case in many nonlinear ceramic capacitors), it may be natural to expect that dark breathers may arise, instead of bright ones. The latter are considerably more technically involved to compute (see, e.g., Ref. [45] and discussion therein) chiefly due to the finite background of the solutions and thus pose a natural challenge towards future work. Additionally, the waveforms examined here, as well as in the earlier work of Ref. [31] have been restricted to one-dimensional settings. Extending consideration to two-dimensional scenarios where the geometry may also play a role (e.g., hexagonal or honeycomb lattices, rather than purely square ones) is then another relevant possibility, especially given recent experimental realizations [46]. Finally, the consideration of composite lattices bearing both right-handed and left-handed elements (see for an example [47]) is another topic of interest in its own right as concerns the nonlinear (numerically exact) breather waveforms that may arise therein. These variants of the present problem are currently under consideration and will be reported in future studies.

Acknowledgments. The authors, V.K., P.G.K., G.P.V., and D.J.F., acknowledge that this work made possible by NPRP grant # [9-329-1-067] from Qatar National Research Fund (a member of Qatar Foundation). The findings achieved herein are solely the responsibility of the authors. We also thank Professor Yannan Shen for numerous useful discussions. V.K. and P.G.K. are grateful for support from the ERC under FP7, Marie Curie Actions, People, International Research Staff Exchange Scheme (IRSES-606096).

---

[1] G. V. Eleftheriades and K. G. Balmain (eds.) *Negative-Refraction Metamaterials. Fundamental Principles and Applications* (John Wiley, New Jersey, 2005).
[2] C. Caloz and T. Itoh, *Electromagnetic Metamaterials: Transmission Line Theory and Microwave Applications* (Wiley, NJ, 2006).
[3] R. Marqués, F. Martín, and M. Sorolla, *Metamaterials with negative parameters. Theory, Design, and Microwave Applications* (John Wiley and Sons, NJ, 2008).
[4] D. R. Smith, W. J. Padilla, D. C. Vier, S. C. Nemat-Nasser, and S. Schultz, Phys. Rev. Lett. **84**, 4184 (2000).
[5] D. R. Smith and N. Kroll, Phys. Rev. Lett. **85**, 2933 (2000); A. Shelby, D. R. Smith, and S. Schultz, Science **292**, 77 (2001).
[6] V. M. Shalaev, Nature Photonics **1**, 41 (2007).
[7] S. Aubry, Physica D **103**, 201 (1997).
[8] S. Flach and A.V. Gorbach, Phys. Rep. **467**, 1 (2008).
[9] M. Sato, B.E. Hubbard, A.J. Sievers, B. Ilic, D.A. Czaplewski and H.G. Craighead, Phys. Rev. Lett. **90**, 044102 (2003).
[10] M. Sato, B.E. Hubbard, L.Q. English, A.J. Sievers, B. Ilic, D.A. Czaplewski and H.G. Craighead, Chaos **13**, 702 (2003).
[11] J. Cuevas, L. Q. English, P. G. Kevrekidis, and M. Anderson Phys. Rev. Lett. **102**, 224101 (2009)
[12] L.Q. English, R. Basu Thakur and R. Stearrett, Phys. Rev. E **77**, 066601 (2008).
[13] E. Trías, J.J. Mazo and T.P. Orlando, Phys. Rev. Lett. **84**, 741 (2000).
[14] P. Binder, D. Abraimov, A.V. Ustinov, S. Flach and Y. Zolotaryuk, Phys. Rev. Lett. **84**, 745 (2000).
[15] U.T. Schwarz, L.Q. English and A.J. Sievers, Phys. Rev. Lett. **83**, 223 (1999).
[16] B. I. Swanson, J. A. Brozik, S. P. Love, G. F. Strouse, A. P. Shreve, A. R. Bishop, W.-Z. Wang, and M. I. Salkola, Phys. Rev. Lett. **82**, 3288 (1999).
[17] N. Boechler, G. Theocharis, S. Job, P.G. Kevrekidis, M.A. Porter and C. Daraio, Phys. Rev. Lett. **104**, 244302 (2010).
[18] C. Chong, F. Li, J. Yang, M. O. Williams, I. G. Kevrekidis, P. G. Kevrekidis, and C. Daraio Phys. Rev. E **89**, 032924 (2014).
[19] N. Lazarides, M. Eleftheriou, and G. P. Tsironis, Phys. Rev. Lett. **97**, 157406 (2006); M. Elefteriou, N. Lazarides, and G. P. Tsironis, Phys. Rev. E **77**, 036608 (2008).
[20] G. P. Tsironis, N. Lazarides and M. Eleftheriou, in: *Nonlinearities in Periodic Structures and Metamaterials*, C. Denz, S. Flach, and Yu. S. Kivshar (eds.), pp. 101-116 (Springer, Berlin, 2009).
[21] A. Grbic and G. V. Eleftheriades, J. Appl. Phys. **92**, 5930 (2002); G. V. Eleftheriades, O. Siddiqui, and A. K. Iyer, IEEE Microwave Wireless Compon. Lett. **13**, 51 (2003).
[22] C. Caloz and T. Itoh, IEEE Trans. Antennas Propagat. **52**, 1159 (2004); A. Lai, C. Caloz, and T. Itoh, IEEE Microwave Magazine **5**, 34 (2004).
[23] A. A. Zharov, I. V. Shadrivov, and Yu. S. Kivshar, Phys. Rev. Lett. **91**, 037401 (2003).
[24] V. M. Agranovich, Y. R. Shen, R. H. Baughman, and A. A. Zakhidov, Phys. Rev. B **69**, 165112 (2004).
[25] M. Lapine, M. Gorkunov, and K. H. Ringhofer, Phys. Rev. E **67**, 065601 (2003).
[26] B. Wang, J. Zhou, T. Koschny, and C. M. Soukoulis, Opt. Express **16**, 16058 (2008).
[27] D. A. Powell, I. V. Shadrivov, and Yu. S. Kivshar, Appl. Phys. Lett. **95**, 084102 (2009).
[28] A. B. Kozyrev and D. W. van der Weide DW, J. Phys. D: Appl. Phys. **41**, 173001 (2008).
[29] J. Ogasawara and K. Narahara, IEICE Electro. Express **7**, 608 (2010).
[30] Z. Wang, Y. Feng, B. Zhu, J. Zhao, and T. Jiang J. Appl. Phys. **107**, 094907 (2010).
[31] Y. Shen, P.G. Kevrekidis, G.P. Veldes, D.J. Frantzeskakis, D. DiMarzio, X. Lan and V. Radisic, "From Solitons to Rogue

Waves in Nonlinear Left-Handed Metamaterials" *to be published.*
[32] C.J.G. Meyers, C.R. Freeze, S. Stemmer, and R.A. York, Applied Physics Letters 109, 112902 (2016)
[33] X. Chen, T. M. Grzegorczyk, B.I Wu, J. Pacheco Jr., and J.A. Kong, Phys. Rev. **70**, 016608 (2004).
[34] M. Beruete, F. Falcone, M.J. Freire, R. Marqués and J.D. Baena, Appl. Phys. Lett. **88**, 083503 (2006).
[35] Macom Technology, "MA46H146 (rev. V5) data sheets," (2016).
[36] R. F. Peierls, Proc. R. Soc. London **52**, 34 (1940); F. R. N. Nabarro, ibid. **59**, 256 (1947).
[37] C. Sulem and P.L. Sulem, *The Nonlinear Schrödinger Equation*, Springer-Verlag (New York, 1999).
[38] M.J. Ablowitz, B. Prinari and A.D. Trubatch, *Discrete and Continuous Nonlinear Schrödinger Systems*, Cambridge University Press (Cambridge, 2004).
[39] P. G. Kevrekidis, D. J. Frantzeskakis, and R. Carretero-González, *The Defocusing Nonlinear Schrödinger Equation*, SIAM (Philadelphia, 2015).
[40] M. Remoissenet, *Waves Called Solitons* (Springer-Verlag, Berlin, 1999).
[41] R.S. MacKay and S. Aubry, Nonlinearity **7**, 1623 (1994).
[42] M. Peyrard, M.D. Kruskal, Physica D **14** 88 (1984).
[43] P. Kevrekidis and M.I. Weinstein Physica D **142**, 113 (2000).
[44] M. Jenkinson, M.I. Weinstein, Nonlinearity **29**, 27 (2016).
[45] C. Chong, P. G. Kevrekidis, G. Theocharis, and Chiara Daraio Phys. Rev. E **87**, 042202 (2013).
[46] L. Q. English, F. Palmero, J. F. Stormes, J. Cuevas, R. Carretero-González, and P. G. Kevrekidis Phys. Rev. E **88**, 022912 (2013).
[47] G. P. Veldes, J. Cuevas, P. G. Kevrekidis, and D. J. Frantzeskakis Phys. Rev. E **88**, 013203 (2013).
[48] R. N. Simons, *Coplanar waveguide circuits, components, and systems* (Wiley, New York, 2001).